



Flow visualization of annular and delta winlet vortex generators in fin-and-tube heat exchanger application

Chi-Chuan Wang^{a,*}, Jerry Lo^b, Yur-Tsai Lin^b, Chung-Szu Wei^a

^a Energy and Resources Laboratories, Industrial Technology Research Institute, Bldg. 64, 195-6 Section 4, Chung Hsing Road, Chutung, Hsinchu, 310, Taiwan

^b Department of Mechanical Engineering, Yuan-Ze University, Taoyuan, Taiwan

Received 16 August 2001; received in revised form 4 February 2002

Abstract

This study presents flow visualization and frictional results of enlarged fin-and-tube heat exchangers with and without the presence of vortex generators. Two types of vortex generators and a plain fin geometry were examined in this study. For plain fin geometry at $Re = 500$, the horseshoe vortex generated by the tube row is not so pronounced, and the horseshoe vortex separates into two streams as it flows across the second row and consequently loses its vortical strength. This phenomenon may support the “maximum phenomenon” in low Reynolds number region reported by previous studies. With the presence of annular vortex generator, the presence of a pair of longitudinal vortices formed behind the tube is seen. The strength of the counter-rotating vortices increases with the annular height and the strength of the longitudinal vortices is so strong that may swirl with the horseshoe vortices and other flow stream. For the same winlet height, the delta winlet shows more intensely vortical motion and flow unsteadiness than those of annular winlet. This eventually leads to a better mixing phenomenon. However, it is interesting to know that the corresponding pressure drops of the delta winlet are lower than those of annular winlet. Compared to the plain fin geometry, the penalty of additional pressure drops of the proposed vortex generators is relatively insensitive to change of Reynolds number. © 2002 Elsevier Science Ltd. All rights reserved.

Keywords: Vortex generator; Fin-and-tube heat exchanger

1. Introduction

Plate fin-and-tube heat exchangers are composed of a plurality of heat transfer tubes that are inserted into respective bores of fins, and are closely fitted and fixed to the latter by means of tube expansion. The fin-and-tube heat exchangers are employed in a wide variety of engineering applications like air-conditioning apparatus, process gas heater, and cooler. In typical applications of the fin-and-tube heat exchangers, the air-side resistance generally comprises over 90% of the total thermal re-

sistance. In this connection, significant efforts were made to improve the airside performance. The first generation of the fin patterns of fin-and-tube heat exchangers is of continuous type such as the plain and wavy fin geometries shown in Fig. 1(a) and (b). This kind of fin-and-tube heat exchanger features relatively reliable and durable performance. However, its comparatively low heat transfer performance boosts the inventions of the second generation of enhanced surfaces such as slit and louver fin geometries (see Fig. 1(c)–(e)). The second generation of interrupted surfaces features enhanced heat transfer mechanisms like boundary layer restarting, wake management, and flow destabilization. A recent patents review by Wang [1] had outlined many of these interrupted fin surfaces.

Despite the fact that interrupted surfaces can significantly improve the heat transfer performance, the

* Corresponding author. Tel.: +886-3-591-6294; fax: +886-3-582-0250.

E-mail address: ccwang@itri.org.tw (C.-C. Wang).

Nomenclature

A_c	cross-sectional area (m ²)	Re	Reynolds number based on channel height (dimensionless)
H_{OV}	height of vortex generator (m)	ΔP_{int}	pressure drops for interrupted surface (Pa)
D	tube outer diameter (m)	ΔP_{Plain}	pressure drops for plain fin geometry (Pa)
D_{VG}	outer diameter of vortex generator (m)	ΔP_{VG}	pressure drops for vortex generator (Pa)
P	periphery of the cross-sectional area (m)	W_{VG}	width of the winlet (m)
R	radius of curvature of the vortex generator of annular winlet (m)	α	angular angle of the vortex generator (deg)

associated penalty of the pressure drop is also tremendous. Thus, in contrast to the commonly interrupted surfaces, the third generation of enhanced surfaces is now receiving a lot of attention. The third generation of the enhanced surfaces employ longitudinal vortex generator that provides swirling motion to the flow field (see Fig. 1(f) of US patent 4817709 [2] that superposed a delta wing on conventional wavy fin surface). Usually the swirling motions may be classified as transverse and longitudinal vortices. The rotation axis of a transverse vortex lies perpendicular to the flow direction while the longitudinal vortices have their axes parallel to the main flow direction. The longitudinal vortex flow may swirl around the primary flow and exhibits three-dimensional characteristics. In general, longitudinal vortices are more effective than transverse vortices from the heat transfer perspective [3]. The imposed vortical motions provide enhanced heat transfer performance with relatively low penalty of pressure drop. This is because wall friction is related to the derivative of streamwise velocity but spanwise and normal velocities. The vortex generators characterized the secondary flow pattern from the vortical motions which are caused by the spanwise and normal velocities. Thus, heat transfer enhancement is associated with the secondary flow but with small penalty of wall friction [4].

The first literature reporting the heat transfer performance improvements is by Edwards and Alker [5]. They reported that the local average heat transfer coefficient was about 40% higher than that of a plain fin surface. For applications to the compact heat exchangers with vortex generators, Fiebig and his co-workers [6–10] had conducted very comprehensive studies in association with the influence of wing type, delta-wing type, delta winlet, and rectangular winlet vortex generators. Very detailed information was reported about these kinds of vortex generators. Fiebig [10] then concluded that the delta winlet shows the best performance. Similar results were also reported by the numerical simulations by Biswas et al. [11], they showed that the flow loss of the winglet-pair is less than that of the wing type. Many investigations were performed to

examine the thermofluid characteristics in compact heat exchanger surface. In the previous investigations, vortex was introduced by imposing vortex generators. However, in practical application of fin-and-tube heat exchanger, additional horseshoe vortices are generated by the presence of the round tube configuration. Thus, the main objective of the present study is to investigate the interactions of these vortices of the imposed vortex generators and the horseshoe vortex. Attempts are made in the feasibility of the annular winlet and delta winlet vortex generators in the applications of fin-and-tube heat exchangers.

2. Experimental Setup

Experiments are performed in a water tunnel as depicted in Fig. 2. As shown in the figure, city water is supplied to the water tank, the water flows through in series to the contraction section, damping screen, the calm section, test section, exit contraction section, flow meter, water pump, and the connection pipe line to complete the cycle. The test section is made of transparent acrylic having a cross section of 254 mm × 15 mm. Flow visualization is performed via dye-injection technique. Five needles that are capable of injecting color dye are placed at the entrance of the inlet section. For further investigating the flow phenomenon inside the heat exchanger, the injection port can be either located in the center or near the wall to keep track of the trajectory behaviors (Fig. 2(b)). Additional dye injection port is placed at the rear of the acrylic tube to observe the flow motion of the inert region behind the tube. A total of seven acrylic test sections were made and tested. Their detailed geometrical parameters and relevant definitions of the vortex generators are shown in Table 1. The test samples include a plain fin configuration and six vortex generators having annular winlet and delta winlet configurations. The tube layouts of the test samples are all staggered. The outer tube diameter is 30.12 mm, and the channel height of the test section is 15 mm. The height of the vortex

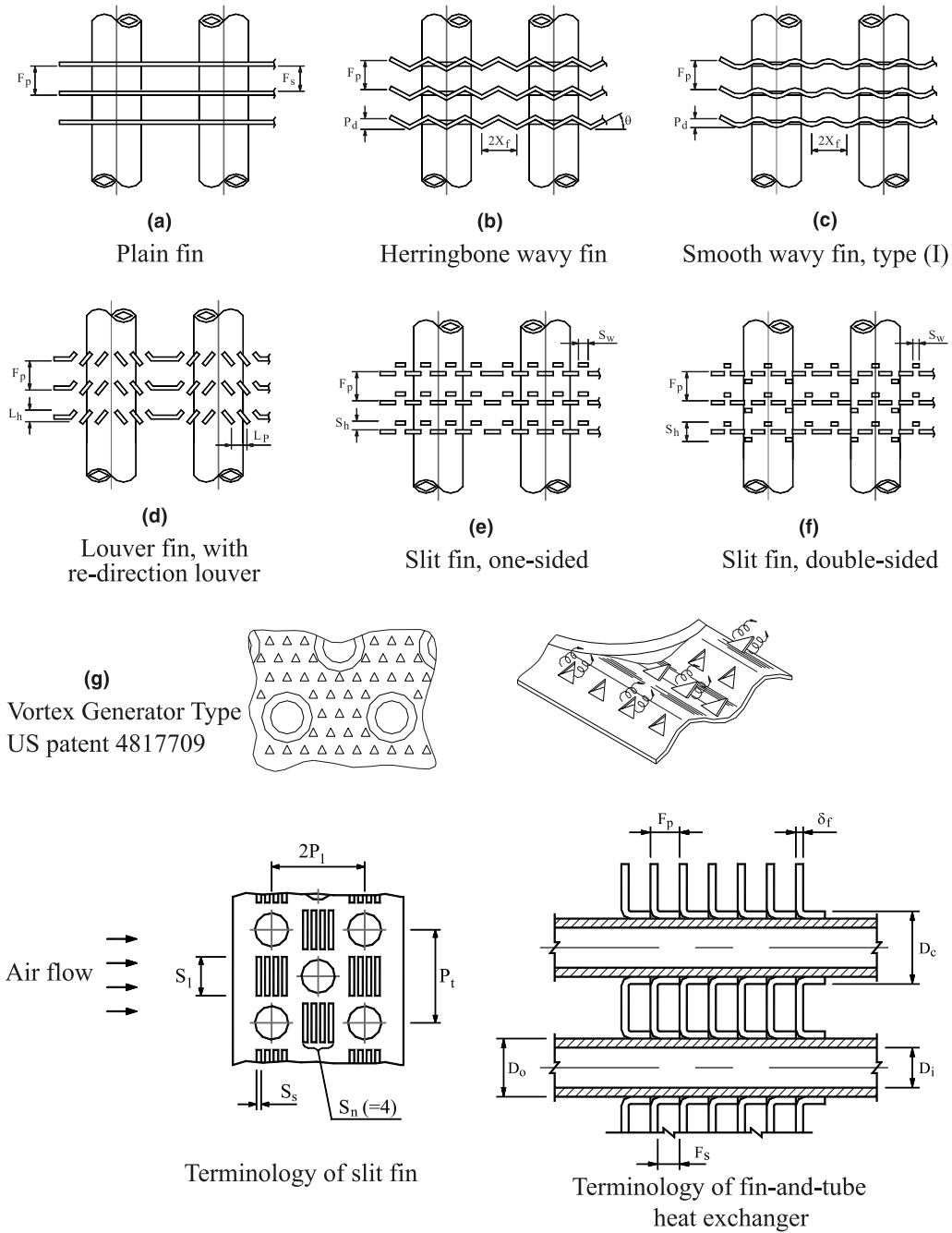


Fig. 1. Various types of vortex generators.

generator H_{VG} varies from 3 to 9 mm, and the corresponding annular diameter D_{VG} is 60.2 mm. Detailed dimension of the vortex generators can also be seen in Table 1.

A digital video camera is placed outside the test section to record the trajectory of the injected dye. The

water flow rate was measured by a very accurate magnetic flowmeter with a calibrated accuracy of 0.002 l/s. The pressure drops across the test section were measured by a precision pressure transducer (YOKOGAWA EJ110). Resolution of this pressure differential pressure transducer is 0.3%. The water temperature inside the

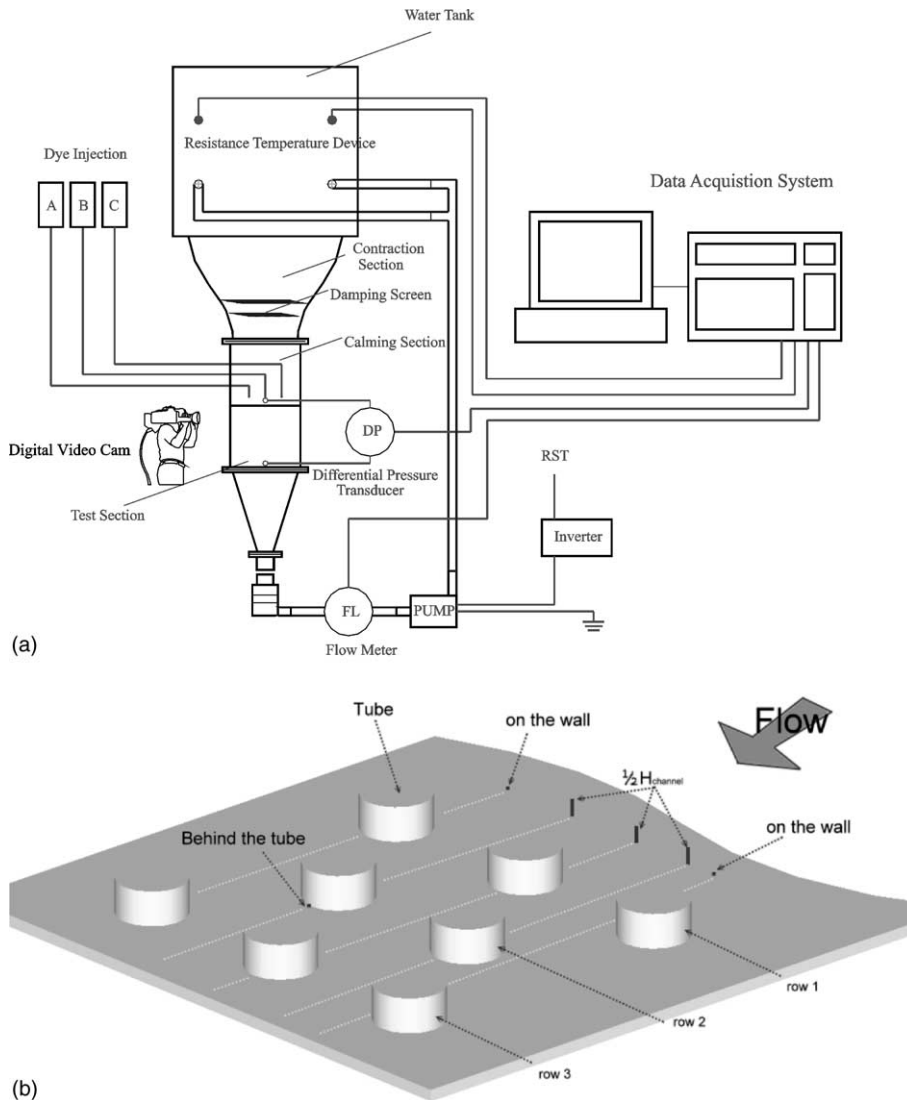


Fig. 2. Schematic of (a) the test facility and (b) the arrangements of the injection port.

tank was measured by resistance temperature device (Pt100 Ω) having a calibrated accuracy of 0.1 $^{\circ}\text{C}$.

3. Results and discussion

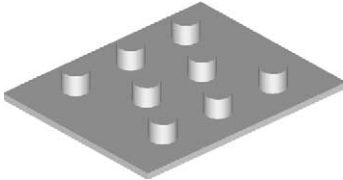
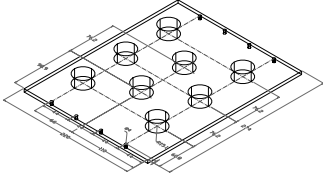
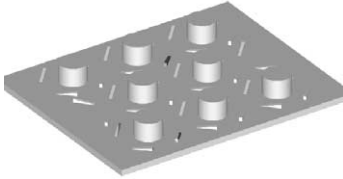
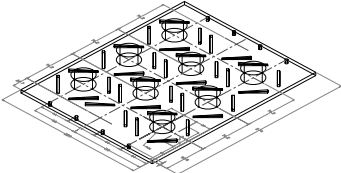
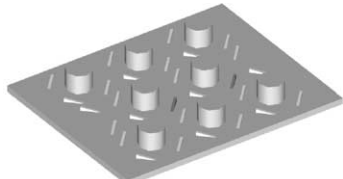
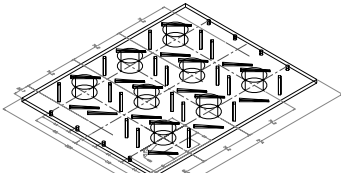
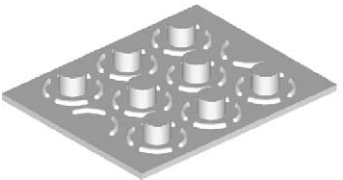
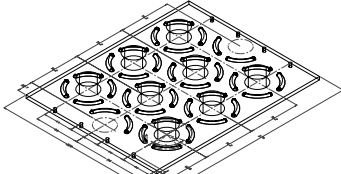
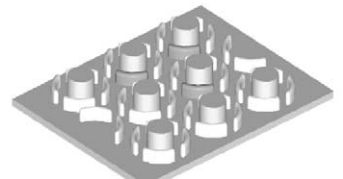
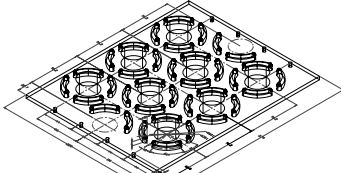

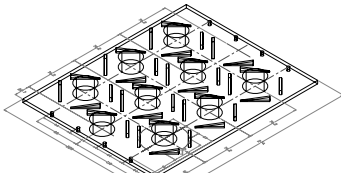
Fig. 3 shows the flow visualization of plain fin geometry with Reynolds numbers of 500, and 1500. The Reynolds number is based on the hydraulic diameter of $4A_c/P$. As shown in Figs. 3(a) and (b), the injected dye in front of the first tube row hits the round tube and twists back a little and then swirls surrounding the round tube to the next and third rows (see Fig. 3(a)). A clear

horseshoe vortex is shown in front of the tube. The strength of the vortical motion that hits the first row is apparently stronger near the first row when comparing to the second and third rows. As the horseshoe vortex is approaching the second row, the flow separated into two streams and the strength of vortical motion is decreased. One of the streams is heading toward the contraction region of the third row and the other is again hitting the third row. However, unlike that in the first row, the stream hitting the third row did not produce a vortical motion, the result implies a drop of heat transfer performance since the swirled motion in front of the tube disappears. The result of the flow motion supports the

test results by Rich [12] and Wang et al. [13] who reported a maximum phenomenon of the Coburn j fac-

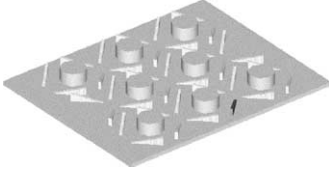
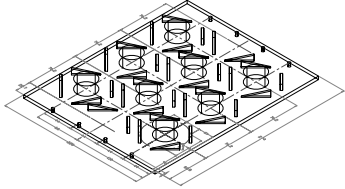
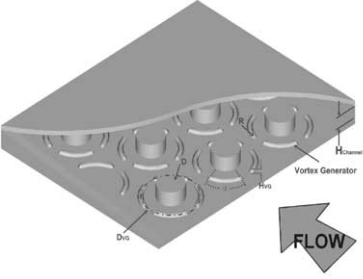
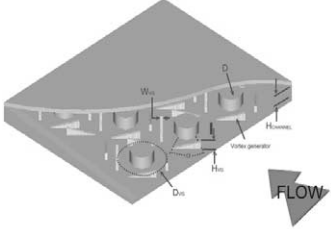
tors vs. Reynolds number at low Reynolds region and larger tube row. Notice that a private discussion between

Table 1
Configuration of the test sample and the definitions of geometrical parameters of vortex generators

Notation	H_{VG} (mm)	R (W_{VG}) (mm)	Schematic	Detailed dimension
SPL (Plain)	/	/		
STVG1	3	3		
STVG2	3	3		
STVG3	3	5.0		
STVG4	6			
STVG5	6	3		

(continued on next page)

Table 1 (continued)

Notation	H_{VG} (mm)	R (W_{VG}) (mm)	Schematic	Detailed dimension
STVG6	9	3		
				

Webb and Rich [14] had attributed this unexpected performance drop phenomenon to the experimental error at low air flow rates. However, one can see that the decrease of the strength of horseshoe vortex may play an important role in this “maximum” flow phenomenon instead of “experimental uncertainty”. The injected dye (blue) right behind the second tube row climbs up the periphery of the tube, and then separated from the tube at an angle of approximate 110° (counting from the stagnation point of the second row). The trajectory of the blue dye then travels along further downstream. It is interesting to note that part of the blue dye then turns around to form a vortex and part of the blue dye flows further downstream to mix with the separated stream from the vortex horseshoe vortex. Axis of the re-circulation vortex is slightly inclined to the flow direction and resembles a transverse vortex. Grosse-Goremann et al. [15] point out that for steady flow conditions transverse vortices do not cause any global enhancement of heat transfer but enhanced friction factor. Thus, this re-circulation zone implies very poor heat transfer characteristics in this region. In addition, the vortex formed behind the tube is quite steady. The shedding frequency of the vortex is quite slow at a Reynolds number of 500 (the period is more than 30 s). Shedding occurs one after another for these two vortices when its size is above a certain limit.

As the Reynolds number is further increased to 1500, one can clearly see in Figs. 3(c) and (d) that the horse-

shoe vortices follow a similar trajectory like $Re = 500$ to the third row. However, unlike that in $Re = 500$, the horseshoe vortex flow does not separate but reveals a unsteady swing as the flow approaches the third row (red dye). In the meantime, the vortex formed behind the second row reveals a detectable periodic shedding and the unsteady swing of the horseshoe vortex in front of the third row is related to the vortex shedding. Notice that there are two vortices formed behind the tube and the sheddings of these two vortices are side-by-side. This flow unsteadiness apparently may improve the heat transfer characteristics. A further increase of the Reynolds number to 2500 as shown in Figs. 3(e)–(f) causes significantly unsteadiness of the flow. One can see that the size of the vortices behind the second row is reduced with an increase of shedding frequency.

With the presence of vortex generator, it may be expected that the flow trajectory may be quite different. In general, the vortical motion becomes more and more pronounced with the height of vortex generator. Fig. 4 shows the typical visual results of $Re = 500$ and 1500 for VG4 geometry. A notable difference is the presence of a pair of longitudinal vortices that forms behind the tube. The strength of the counter-rotating vortices is quite strong and, as clearly seen in the figure, the rotational radius of the longitudinal vortices decreases along the streamwise direction. This implies the flow speeds up in the streamwise direction. The strong swirled motion apparently spirals the nearby fluids for better mixing

characteristics. As a consequence, the heat transfer performance is expected to be improved as compared to

that of the plain fin geometry. This phenomenon can be made clear from the trajectory of the red dye from

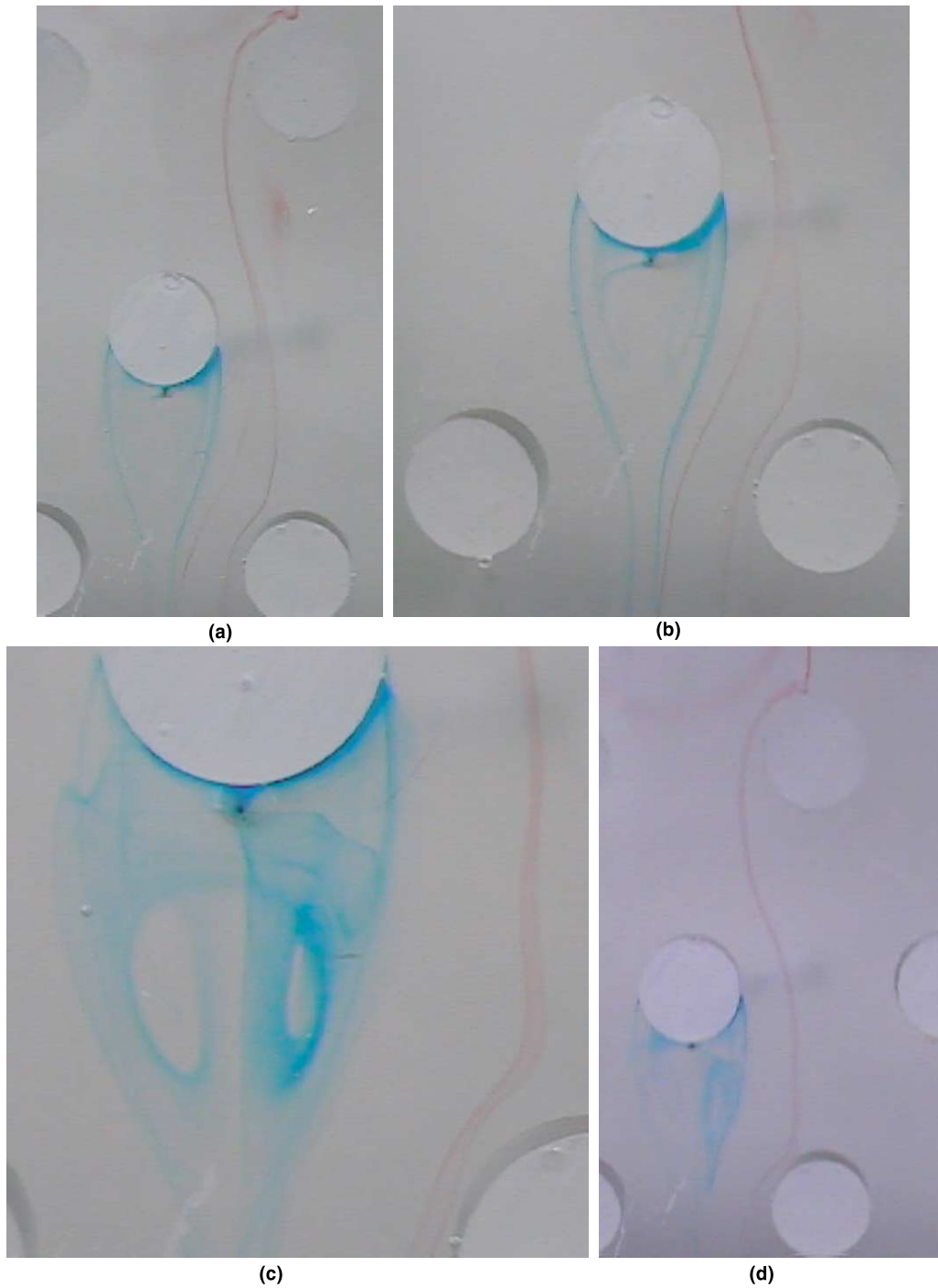


Fig. 3. Flow visualization of the plain fin geometry at (a), (b) $Re = 500$, red dye injected at the center, (c), (d) $Re = 1500$, and (e), (f), (g) $Re = 2500$.

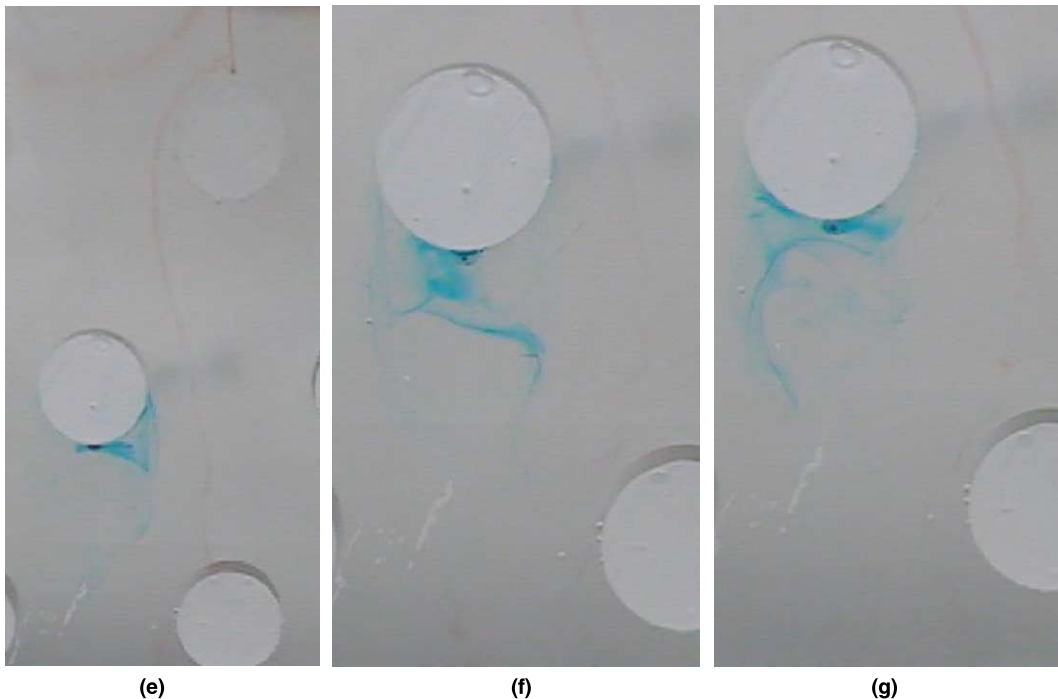


Fig. 3 (continued)

Figs. 4(a) and (b). For the injection port located at the wall (the trajectory of the red dye at the right-hand side of Fig. 4(a)), one can see the fluid trajectory that flows around the first vortex generator and continues to the second vortex generator. Because of the strong vortex flow formed behind the tube row (see Fig. 4(c)), the flow is swirled into the back of the tube and reveals a vortical motion which then flips over the vortex generator when the blue dye was flows across the second row. On the other hand, the red dye (injected in the center part at the entrance) that flows over the first generator also reveals a swirled motion. Although the swirled motion is not so pronounced as that formed behind the tube (the second blue dye trajectory from the right-hand side of Fig. 4(a)), but the longitudinally rotated motion persists quite further downstream without breaking up. As shown in Figs. 4(a) and (c), for the red dye hitting the tube, the horseshoe vortex prevails its vortical motion from first row to the third row without breaking up at $Re = 500$. In addition, the horseshoe vortex hitting the first row will generate counter-rotating vortices, and the flow hits the first vortex generator also generates a pair of counter-rotating vortices. The pair of vortices will change their rotating direction when they flow across the second pair of vortex generator in the downstream. In summary, the rotating direction reversed where vortex generators met. Visual results for $Re = 1500$ of STVG4

are seen for Figs. 4(d)–(f). In a general description, the swirled motion behind the tube becomes even more pronounced as the Reynolds number is increased. As a result, other flow trajectory may swirl with the strongly vortical motions and reveals an early transition to turbulence. The results are analogous to previous investigators that reported an early transition to turbulence with the presence of vortex generator.

Similar visual results were obtained for vortex generator having delta winlet configuration (Fig. 5) but with a much more pronounced vortical motions in every part of the injection port. In general, the swirled motions of the delta winlet configurations are more intense than those of previous annular winlet. Notice that the present annular winlet configuration is similar to that of a rectangular winlet. Fibig [10] indicated that the heat transfer performance for delta winlet is better than that of rectangular winlet. The results can be made clear from the presence of flow unsteadiness caused by the delta winlet. Even at a low Reynolds number of 500, one can see a strong mixing of the blue dye and part of the red dye (Fig. 5(b)). Note that the red dye is the horseshoe vortex from the first row. This phenomenon is not clearly seen for the annular winlet. Further, as can be seen by the self-sustained flow oscillation if the Reynolds number is further increased to 1500 this phenomenon is much more pronounced than that of the annular winlet.

In summary, the observed flow behaviors, with and without the presence of vortex generator, can be roughly

described by Fig. 6. The horseshoe vortex that hits the first row will generate counter-rotating vortices, and the

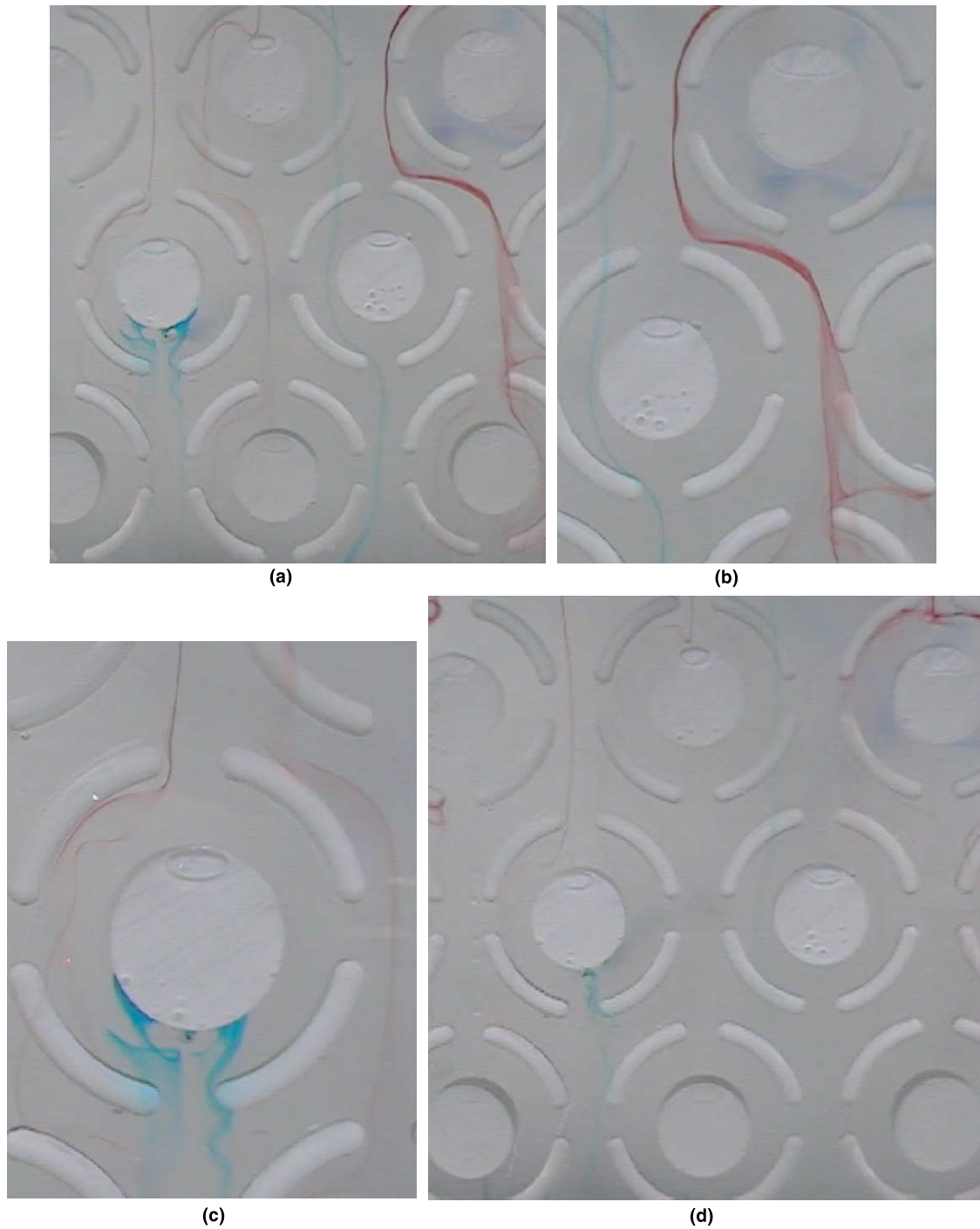


Fig. 4. Flow visualization of the STVG4 vortex generator at (a)–(c) $Re = 500$ and (d)–(f) $Re = 1500$.

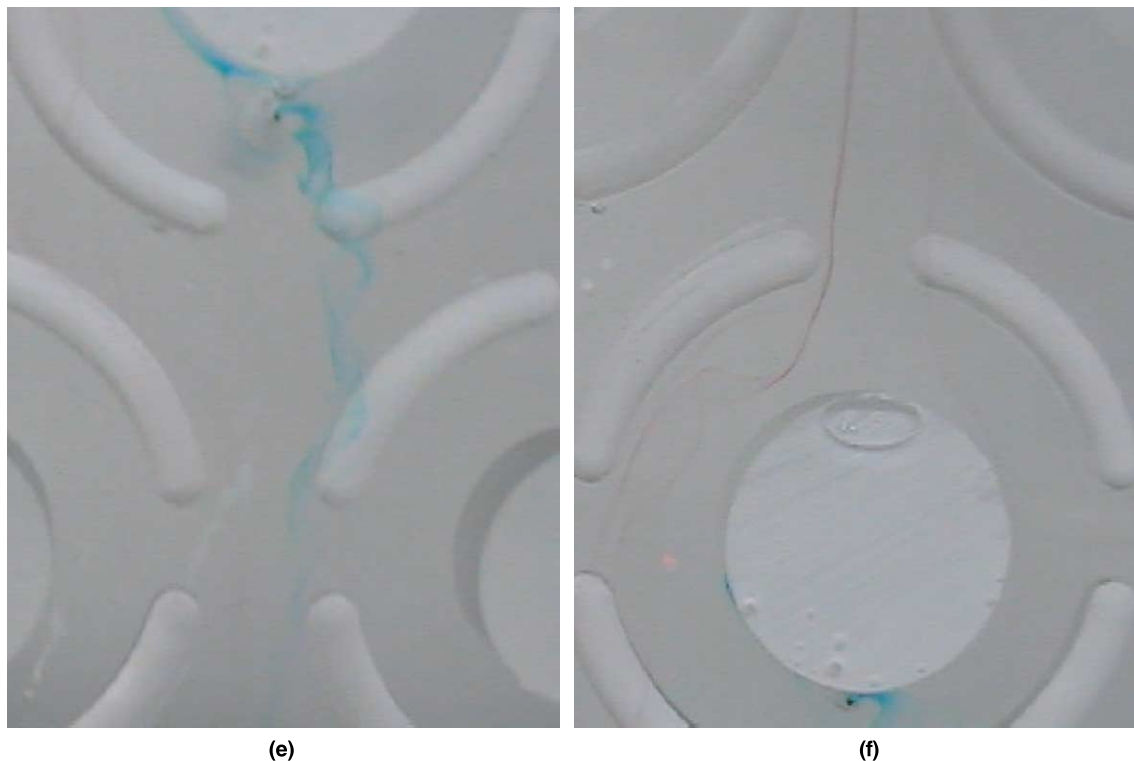


Fig. 4 (continued)

flow hitting the first vortex generator also generates a pair of counter-rotating vortices. The pair of vortices will change their rotating direction when they flow across the second pair of vortex generator in the downstream. In addition, increase of the winlet height will intensify the vortical and unsteady flow characteristics for both annular and delta winlets. However, one can see that the vortical motion of the delta winlet is more intense than that of the annular winlet. The corresponding pressure drops of the vortex generators and the plain fin geometry are shown in Fig. 7. As shown in the figure, depending on the height of the winlet, the pressure drops of the vortex generators exceed those of plain fin geometry by approximately 10–65%. The penalty of pressure drops of the proposed vortex generators to the plain fin geometry is relatively insensitive to change of Reynolds number. This is quite different from those interrupted surfaces that often show consecutive increase of $\Delta P_{\text{int}}/\Delta P_{\text{plain}}$ vs. Reynolds number [16]. By examination of the pressure drops of the annular winlet and the delta winlet at the same Reynolds number, it is interesting to know that the corresponding pressure drop of the delta winlet is lower than that of the annular winlet. Further, the vortical motions and mixing char-

acteristics of the delta winlet are better than those of the annular winlet configuration. Although no heat transfer data were reported in this study, the flow patterns and the frictional performance of the delta winlet vortex generators show promising prospective.

4. Conclusions

This study presents flow visualization and frictional results of enlarged fin-and-tube heat exchangers with and without vortex generators. Two types of vortex generators and a plain fin geometry were examined in this study. The vortex generators investigated in this study are the annular winlet and the delta winlet. Tests are performed in a water tunnel by utilizing dye-injection technique. Major conclusions of this study are summarized as follows:

- (1) For plain fin geometry at $Re = 500$, the horseshoe vortex generated by the tube row is not so pronounced, and the horseshoe vortex separates into two streams as it flows across the second row. The vortical strength loses its momentum considerably.

This phenomenon may support the “maximum phenomenon” in the low Reynolds number region reported by previous studies.

(2) For plain fin geometry at $Re = 1500$, unlike that in $Re = 500$, the horseshoe vortex flow does not separate but reveals an unsteady swing as the flow

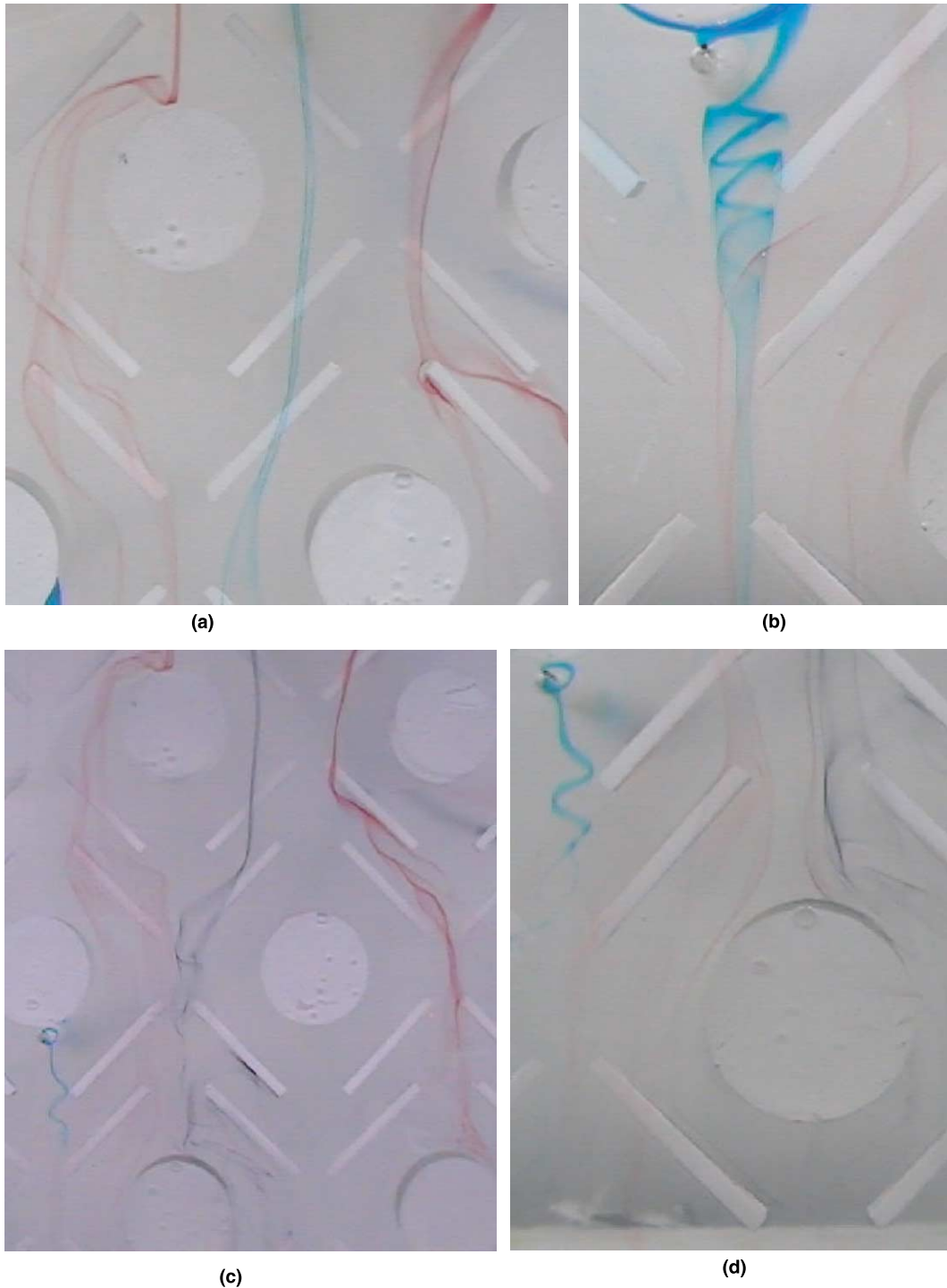


Fig. 5. Flow visualization of the STV5 vortex generator at (a), (b) $Re = 500$ and (c), (d) $Re = 1500$.

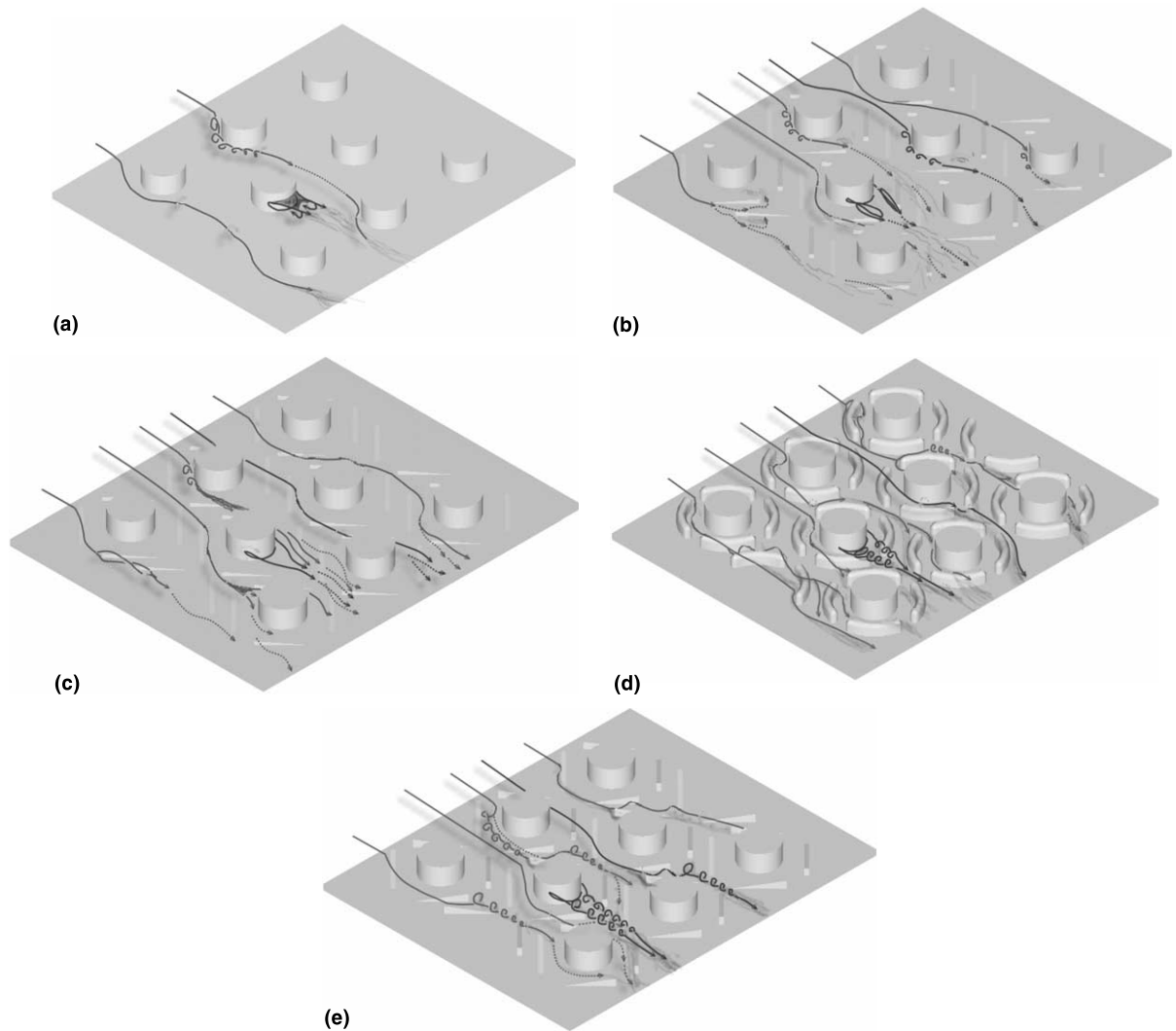


Fig. 6. Schematic of the flow motions across the vortex generators. (a) $Re = 1000$, STPL; (b) $Re = 1000$, STVG1; (c) $Re = 1000$, STVG2; (d) $Re = 1000$, STVG4; (e) $Re = 1000$, STVG5.

approaches the third row. In the meantime, the vortex formed behind the second row reveals a detectable periodic shedding and the unsteady swing of the horseshoe vortex is related to the vortex shedding.

- (3) With the presence of the annular vortex generator, one can see a pair of longitudinal vortices that formed behind the tube. The strength of the counter-rotating vortices increases with the annular height. The strength of the longitudinal vortices is so strong that may swirl with the horseshoe vortices and other flow stream.
- (4) For the same winlet height, the delta winlet shows more intensely vortical motion and flow unsteadiness. This eventually leads to a better flow mixing phenomenon. However, it is interesting to know that

the corresponding pressure drops of the delta winlet are lower than those of the annular winlet at the same Reynolds number.

- (5) The frictional penalty of the proposed vortex generators is about 10–65% higher than that of the plain fin geometry. The penalty of pressure drops of the proposed vortex generators to plain fin geometry is relatively insensitive to change of Reynolds number.

Acknowledgements

The authors would like to express gratitude for the Energy R&D foundation funding from the Energy Commission of the Ministry of Economic Affairs, Taiwan.

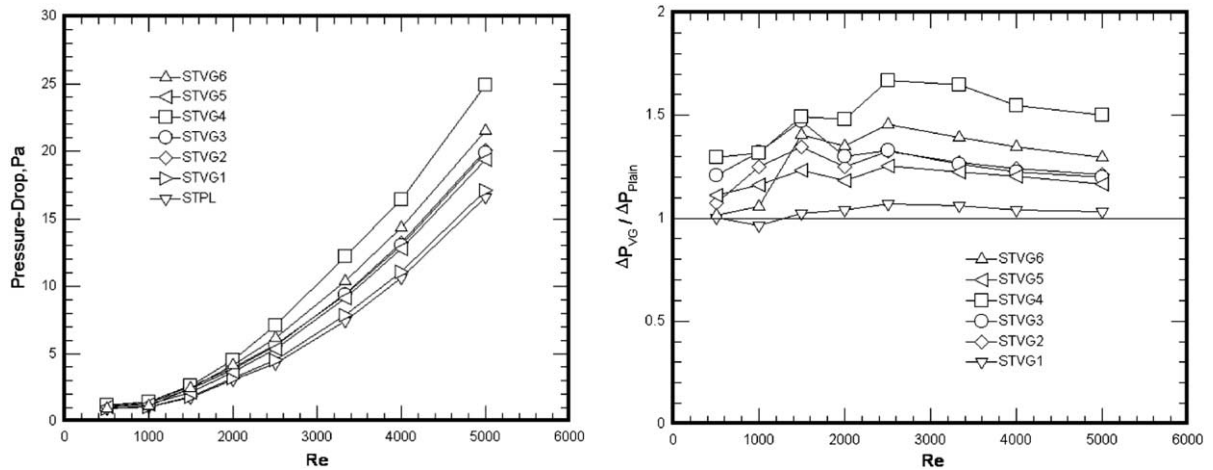


Fig. 7. Frictional performance for the plain fin geometry and vortex generators.

References

- [1] C.C. Wang, Technology review – a survey of the recent progress of the patents of fin-and-tube heat exchangers, *J. Enhanced Heat Transfer* 7 (2000) 333–345.
- [2] J.L. Esformes, Ramp wing enhanced plate fin, US patent 4817709, 1989.
- [3] M. Fibig, Vortices and heat transfer, *ZAMM Z. Angew Math. Mech.* 77 (1) (1997) 3–18.
- [4] A.M. Jacobi, R.K. Shah, Heat transfer surfaces enhancement through the use of longitudinal vortices: a review of recent progress, *Exp. Thermal Fluid Sci.* 11 (1995) 295–309.
- [5] F.J. Edwards, G.J.R. Alker, The improvement of forced convection surface heat transfer using surface protusions in the form of (A) cubes and (B) vortex generators, in: *Proceedings of the 5th International Heat Transfer Conference, Tokyo, vol. 2, 1974*, pp. 244–248.
- [6] M. Fibig, P. Kallweit, N.K. Mitra, S. Tiggelbeck, Heat transfer enhancement and drag by longitudinal vortex generators in channel flow, *Exp. Thermal Fluid Sci.* 4 (1991) 103–114.
- [7] S. Tiggelbeck, N.K. Mitra, M. Fibig, Flow structure and heat transfer in a channel with multiple longitudinal vortex generators, *Exp. Thermal Fluid Sci.* 5 (1992) 425–436.
- [8] S. Tiggelbeck, N.K. Mitra, M. Fibig, Experimental investigations of heat transfer enhancement and flow losses in a channel with double rows of longitudinal vortex generators, *Int. J. Heat Mass Transfer* 36 (1993) 2327–2337.
- [9] S. Tiggelbeck, N.K. Mitra, M. Fibig, Comparison of wing-type vortex generators for heat transfer enhancement in channel flows, *J. Heat Transfer* 116 (1994) 880–885.
- [10] M. Fibig, Vortices, generators and heat transfer, *Trans. IChemE* 76 (Part A) (1998) 108–123.
- [11] G. Biswas, P. Deb, S. Biswas, Generation of longitudinal streamwise vortices – a device for improving heat exchanger design, *ASME J. Heat Transfer* 116 (1994) 588–597.
- [12] D.G. Rich, The effect of the number of tube rows on heat transfer performance of smooth plate fin-and-tube heat exchanger, *ASHRAE Trans.* 81 (1) (1975) 307–317.
- [13] C.C. Wang, Y.J. Chang, Y.J. Hsieh, Y.T. Lin, Sensible heat transfer characteristics of plate fin-and-tube heat exchangers having plane fins, *Int. J. Refrigeration* 19 (4) (1996) 223–230.
- [14] D.L. Gray, R.L. Webb, Heat transfer and friction correlations for plate finned-tube heat exchangers having plain fins, in: *Proceedings of the 8th Heat Transfer Conference, 1986*, pp. 2745–2750.
- [15] A. Gross-Goremann, W. Hahne, M. Fiebig, Influence of rib height on oscillations, heat transfer, and pressure drop in Laminar channel flow, in: *Proceedings of the Eurotherm 31 “Vortices and Heat Transfer”, Bochum, Germany, 1993*, pp. 36–41.
- [16] C.C. Wang, C.J. Lee, C.T. Chang, Some aspects of the fin-and-tube heat exchangers: with and without louvers, *J. Enhanced Heat Transfer* 6 (1999) 357–368.